Crystallization kinetics of $Fe_{40}Ni_{38}Mo_4B_{18}$ and $Fe_{80}B_{20}$ metallic glasses

F. L. CUMBRERA, H. MIRANDA, A. CONDE, R. MÁRQUEZ
Departamento de Optica y Sección de Física del Centro Coordinado del C.S.I.C., Universidad de Sevilla, Spain

P. VIGIER
Groupe de Métallurgie Physique, Faculté des Sciences de Rouen, France

Experimental results for magnetic susceptibility, calorimetry and electrical resistivity for the metallic glasses 2826 MB ($Fe_{40}Ni_{38}Mo_4B_{18}$) and 2605 ($Fe_{80}B_{20}$) are reported. The crystallization kinetics of these alloys is investigated and activation energies are estimated. Time variation of crystallized fraction derived from isothermal electrical runs is interpreted to give the preponderant mechanisms involved in the crystallization process.

1. Introduction

There is considerable interest in amorphous metal systems, particularly those of the Metglas type. A combination of remarkable soft-magnetic, mechanical and electrical properties are shown by these alloys and it is well known that their physical properties are inherently structure-sensitive. The metastable amorphous structure is always tending toward more stable structures through the irreversible relaxation processes, and changes in physical properties can be noticeable. In particular, such properties undergo drastic changes when crystallization occurs. Thus, it is important to study the process of crystallization because it is essential for understanding the effects of crystallization on observed properties. Detailed studies of physical properties and crystallization behaviour are lacking for the 2826 MB ($Fe_{40}Ni_{38}Mo_4B_{18}$) alloy. For the 2605 ($Fe_{80}B_{20}$) system, extensive studies have recently been reported but there is some uncertainty about its crystallization behaviour, and over relations between kinetic parameters and structural changes. Crystallization of these systems has been studied by the authors by conventional transmission electron microscopy and high voltage electron microscopy [1].

The present paper deals with magnetic susceptibility, calorimetric and electrical measurements of these alloys, and a kinetic study leading to an interpretation of the crystallization process, in agreement with the electron microscopy results, is reported.

2. Experimental results

Glassy ribbons of Metglas 2826 MB and 2605 were supplied by the Allied Chemical Corporation, Morristown, New Jersey. Low-field magnetic susceptibility measurements were performed in a nitrogen atmosphere using a Faraday balance magnetometer and a heating rate of 8 K min^{-1}.

Calorimetric measurements were carried out by DTA and DSC techniques with a constant heating rate in the range 2−64 K min^{-1}. The mass of each sample was properly chosen for every heating rate in order to avoid the self-heating phenomenon. The melting of several milligrams of Pb and Zn was used to calibrate both temperature and enthalpy scales.

For electrical measurements, samples of about 0.5 cm long were cut from received ribbons. The electrical resistivity of the samples was determined by standard d.c. four-probe techniques: the van der Pauw method [2] for Metglas 2826 MB, and the Valdés method [3] for Metglas 2605. Different thermal treatments were done: dynamic heating (up to 875 K) at several rates, and isothermal annealing at different temperatures below the crystallization temperature. Electrical measurements in the course of thermal treatments were carried out in a vacuum chamber ($\simeq 10^{-2}$ Pa).

© *1982 Chapman and Hall Ltd.*

3. Results

3.1. Magnetic susceptibility

Fig. 1 shows the low-field susceptibility of Metglas 2826 MB as a function of temperature, T. Curie temperatures, T_c, were found by extrapolating the χ^2 against T straight line, running through the rapidly diminishing experimental points to $\chi = 0$. This method has been extensively employed [4–6]. For the as-received samples, T_c is 617 ± 5 K. Details of the temperature variation in the range 700–800 K can be observed in the amplified view included in Fig. 1. Increases in χ reveal that crystallization occurs by a two-step process at temperatures of 700 and 725 K. Measurements carried out after annealing for 2 h at 1000 K (dashed line) show two magnetic crystalline phases with Curie points $T_{c1} = 560$ K and $T_{c2} = 690$ K, respectively. These results agree with previously reported data [7] except for the T_{c2} temperature, which is significantly higher (755 K) in that paper.

In Fig. 2 we have plotted susceptibility against T for Metglas 2605. In the heating cycle we get $T_c = 665 \pm 5$ K (this high Curie point is a characteristic of Metglas 2605). As observed, crystalliz-

ation takes place at 700 K in a narrower temperature range than for the other Metglas. After crystallization, a magnetic phase with a Curie point 845 K can be observed, and annealing for 2 h at 1000 K shifts this point to 800 K. This shift of Curie point provides evidence of the metastable character of the crystal structure obtained at 700 K in spite of stabilization for 2 h carried out at this temperature. The Curie point of 815 K can be assigned to the Fe_3B compound, formed simultaneously with the α-Fe through a eutectic transformation in the first stage of crystallization [8–10]. For higher temperatures, Fe_3B transforms to α-Fe + Fe_2B and the final Curie point of 800 K should correspond to the stable Fe_2B phase.

3.2. Electrical resistivity

The temperature dependence of electrical resistivity for 2826 MB and 2605 alloys is plotted in Figs 3 and 4, respectively. No changes in the qualitative features of the plots with heating rate have been observed. For both materials, an approximately linear variation of ρ against T in the range room temperature to 550 K is observed, and least-
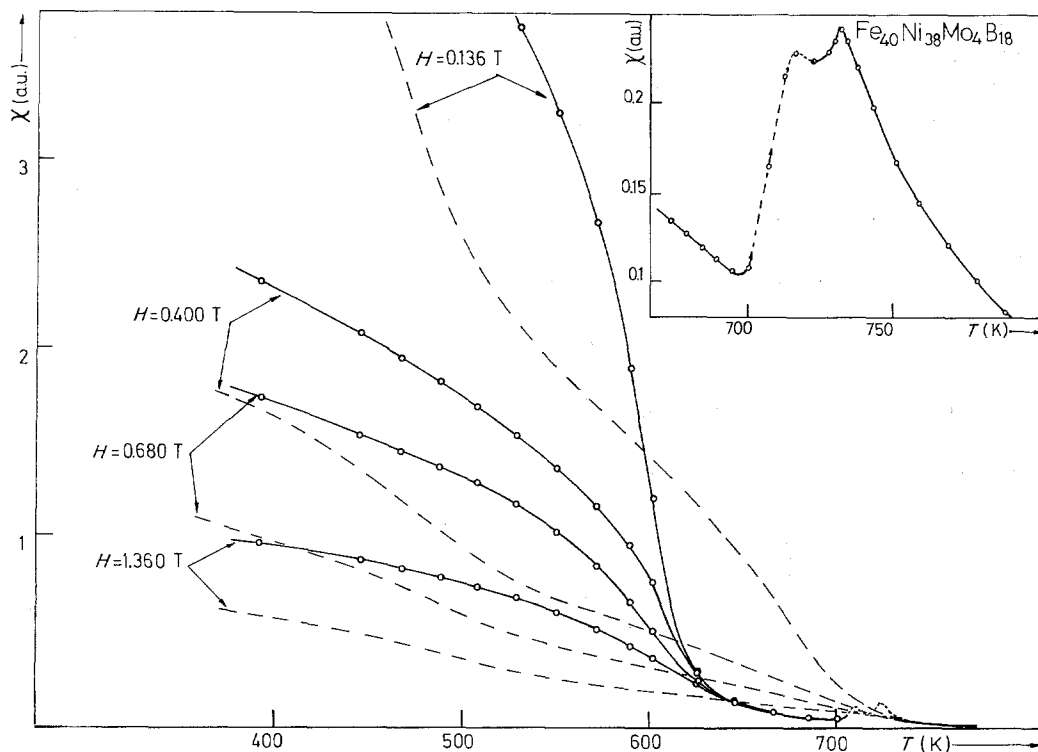
Figure 1 Magnetic susceptibility of 2826 MB alloy as a function of temperature: as-received (continuous line) and after annealing (dashed line). The enlarged view shows the details of crystallization range.
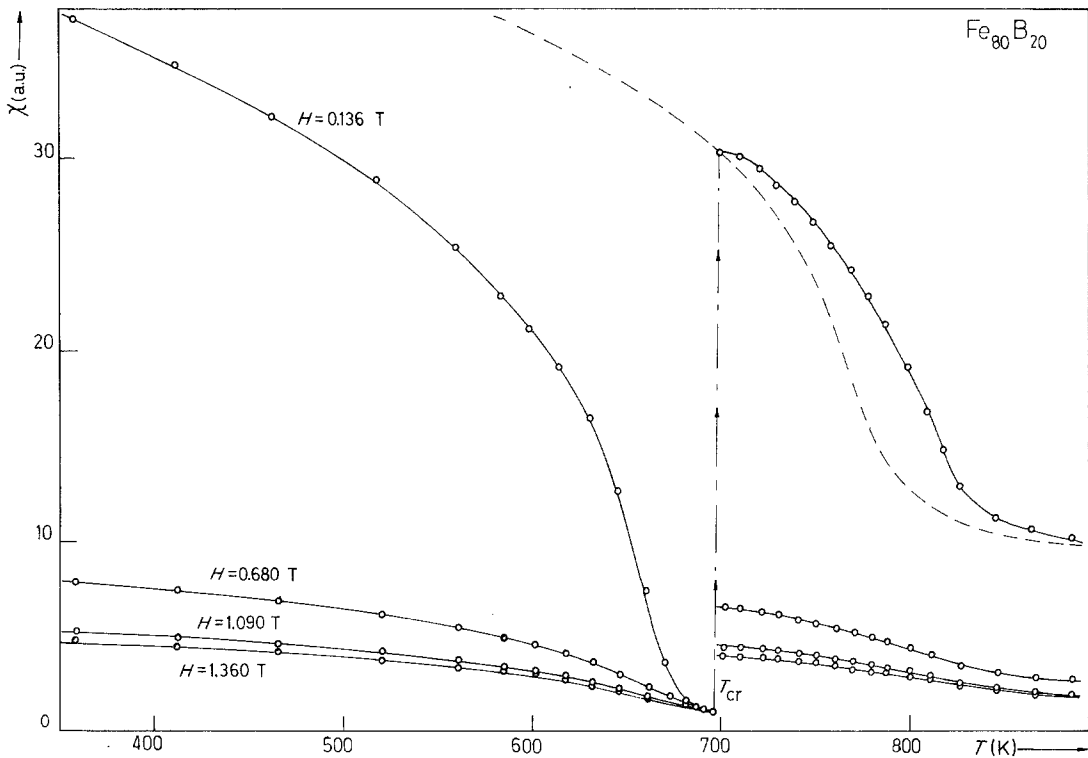
Figure 2 Magnetic susceptibility of 2605 Metglas. Dashed line corresponds to the sample annealed at 1500 K.

squares fitting to the expression: $\rho(T) = \rho_0(1 + \alpha T)$ gives the values $\rho_0 = 151.3\,\mu\Omega\,cm$, $\alpha = 4.5 \times 10^{-5}\,K^{-1}$ for 2826 MB alloy, and $\rho_0 = 115.5\,\mu\Omega\,cm$, $\alpha = 7.9 \times 10^{-5}\,K^{-1}$ for 2605 alloy. The small positive TCR observed, agrees with previous results [11] and with the value $(\alpha \sim 10^{-4}\,K^{-1})$ predicted by Ziman for metallic amorphous alloys above the Debye temperature. The Curie point, revealed as an anomaly in $d\rho/dT$, is detected for both materials [10].

As observed in Fig. 3, the ρ against T curve clearly shows that crystallization in Metglas 2826 MB consists of at least two steps. The crystallization starts close to 700 K at which temperature
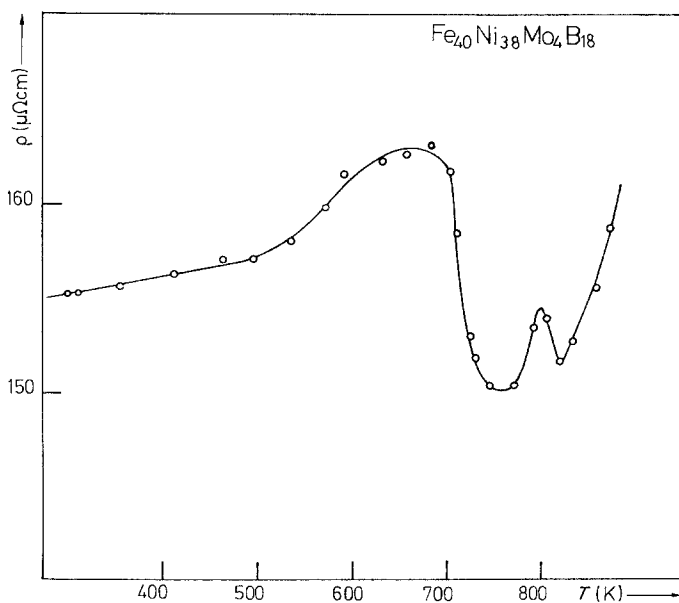
Figure 3 Plot of electrical resistivity against temperature for 2826 MB Metglas.

2679
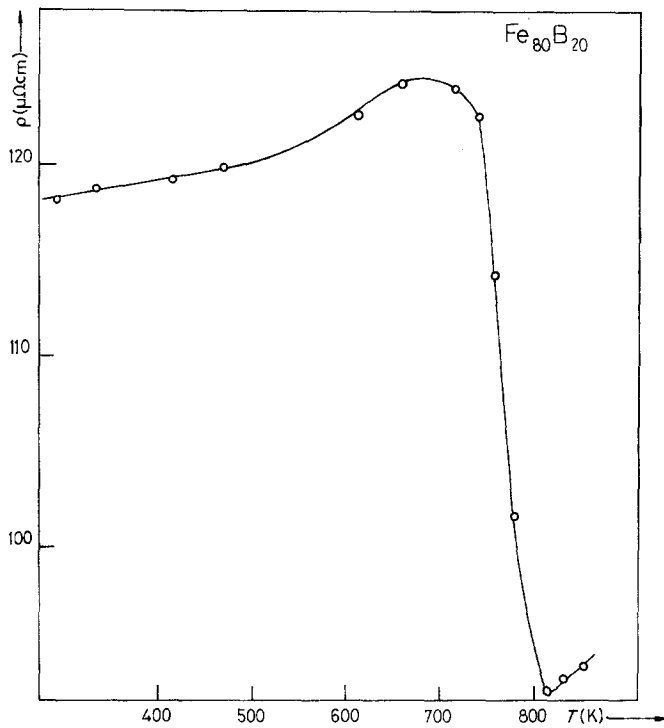
Figure 4 Plot of electrical resistivity against temperature for 2605 Metglas.

the electrical resistivity begins to decrease by $\sim 13\,\mu\Omega\,\text{cm}$. The second stage of crystallization takes place near 810 K and is characterized by a $\sim 3\,\mu\Omega\,\text{cm}$ drop in ρ.

Fig. 4 shows that the resistivity of Metglas 2605 changes discontinuously at the crystallization temperature and a sharp drop of $\sim 32\,\mu\Omega$ cm is observed. This resistivity change upon crystallization is similar to those observed for $Fe_{30}(B_{1-x}P_x)_{20}$ amorphous alloys [12].
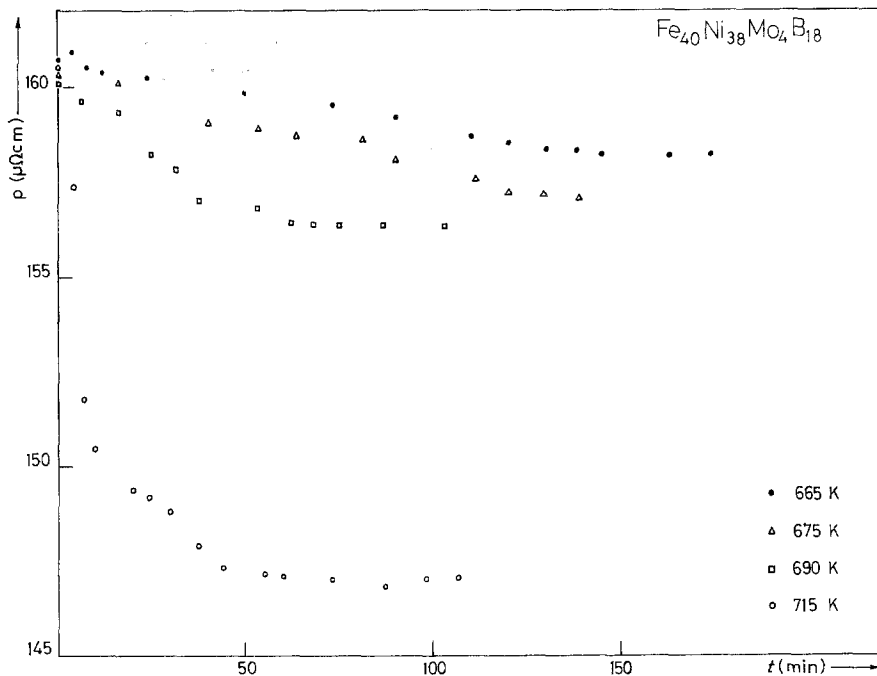
Figure 5 Time dependence of electrical resistivity at various annealing temperatures for 2826 MB Metglas.

The time-dependence of the electrical resistivity at various annealing temperatures is presented in Figs 5 and 6 for 2826 MB and 2605 alloys. In the plots, zero time corresponds to initial stabilization after a small induction time, below 10 min, in all cases. An observable feature in some of the isothermal annealing data is the presence of an initial transient where the resistivity increases prior to decreasing with annealing time as crystallization proceeds. This transient was most noticeable at the lower annealing temperatures. For annealing temperatures near the onset of crystallization, an initial sharp drop is observed and the time required to approach the asymptotic value is shorter than at lower temperatures. TEM observations [1] allow us to justify these results. A remarkable difference exists between crystallization processes taking place through isothermal annealings near the crystallization temperature and those occurring at lower temperatures.

In terms of the Johnson–Mehl–Avrami equation [13] the transformed fraction $x(t)$ is:

$$x(t) = 1 - \exp{(-t/\tau)^n}$$

where τ is the time constant and n the Avrami exponent. The time constant is usually approximated by an Arrhenius-type temperature, T, dependence

$$\tau = \tau_0 \exp{(-E/kT)}$$

where k is the Boltzmann constant, E is the apparent thermal activation energy, and τ_0 is the time factor. Experimental data provide $n \log \tau$ for different temperatures, and then a plot of this magnitude against $1/T$ provides an estimation of the activation energy. Values of $2.1 \, \text{eV at}^{-1}$ and $2.3 \, \text{eV at}^{-1}$, respectively, have been obtained for the activation energy in 2826 MB and 2605 alloys.

4. Crystallization kinetics
In this section a kinetic study of crystallization based on calorimetric and electrical measurements is reported.

4.1. Calorimetry
DTA results for the 2826 MB alloy reveal three stages in the crystallization, in agreement with recently reported results [7]. In our case, exothermic peaks occur at around 725, 815 and 875 K, but it should be noted that these temperatures depend on the heating rate. Crystallization enthalpies of 31, 86 and $14 \, \text{J g}^{-1}$, respectively, have been found. The second peak is enlarged at the low-temperature side and this effect increases with the heating rate. The glass transition is detected at the higher heating rates.

For Metglas 2605 a single exothermic peak in
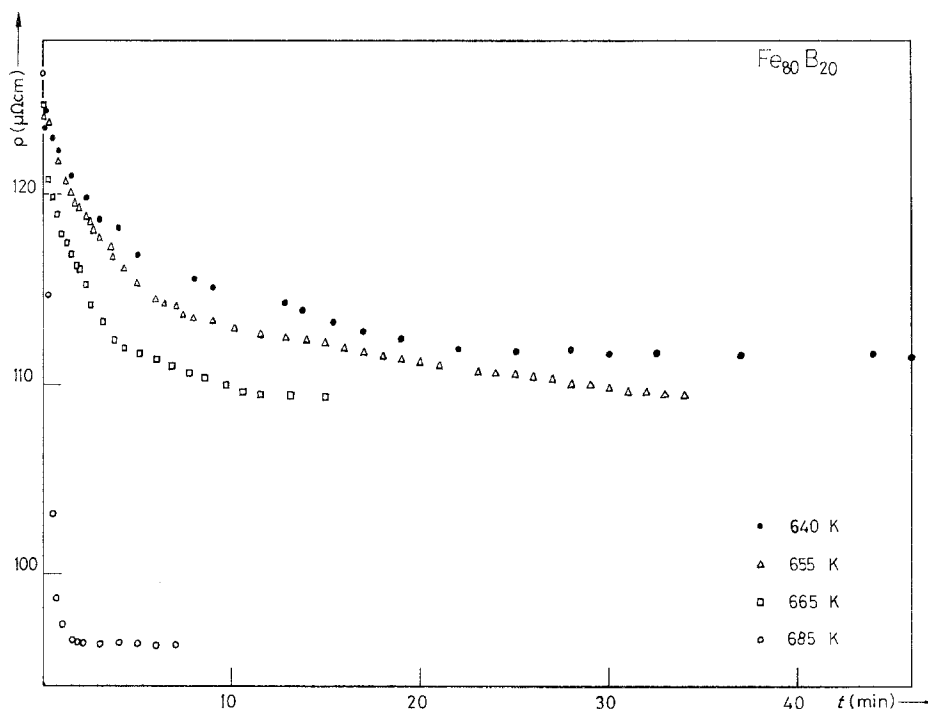
Figure 6 Time dependence of electrical resistivity at various annealing temperatures for 2826 MB.

the crystallization range is detected at around 710K, and the calculated enthalpy is 268 J g^{-1}. The Curie point is detected by a shift of the base line in the endothermic direction.

Kinetic studies have been carried out frequently by means of isothermal measurements, but it has been shown previously [14, 15] that metallic systems are particularly suitable for non-isothermal studies because of their high thermal conductivity. Non-isothermal runs were used in the present study.

The temperature dependence of the crystallized fraction, x, for both materials is plotted in Fig. 7 and the typical sigmoidal form is observed. Curves (a) and (b) are obtained from first and second peaks of the 2826 MB thermogram; curve (c) corresponds to the single peak in the 2605 alloy. A classical method of obtaining an activation energy for a crystallization process is based on the kinetic relation:

$$ dx/dt = K(T)f(x) \quad \text{with} \quad f(x) = (1-x)^{n}. $$

$K(T)$ is temperature dependent according to an Arrhenius expression; the possible values for n being: $0, \frac{1}{2}, \frac{2}{3}$ and 1, depending on the proposed mechanism [13]. The equation to solve is:

$$ dx/dT = A/\beta \cdot f(x) \cdot e^{-E/KT}, $$

with A the pre-exponential factor and β the heating rate. Values obtained for activation energy are 3.0 and 4.7 eV at^{-1}, respectively, for the first

and second peaks of the 2826 MB alloy and 1.7 eV at for the 2605 Metglas.

Another way to evaluate the activation energy is based on the Kissinger formula [16]

$$ \ln\left(\frac{\beta}{T_m^2}\right) = -\frac{E}{KT_m} $$

relating T_m, temperature of the maximum crystallization rate, and β, the heating rate. Values of activation energy obtained by this method are 3.0 and 3.7 eV at^{-1} for 2826 MB alloy peaks and 2.0 eV at^{-1} for 2605 alloy, in satisfactory agreement with the above results. Differences between these values of activation energies and those obtained from electrical measurements through isothermal annealing could be explained as a consequence of different characteristics of the crystallization process under isothermal annealing and dynamic treatment, as reported in our TEM study [1].

The dispersion in values of activation energies obtained from calorimetric analysis can be assigned to different reasons, as explained by Leake and Greer [17]: non-uniformity of specimens and the temperature lag between sample and sample holder.

Activation energies obtained in this way, refer to the whole process of crystallization, including nucleation and growth mechanisms [18, 19]. A study of both contributions to activation energy is contemplated at present by quantitative TEM.

It is worthwhile to compare 2826 MB activation energies with those of the also complex system
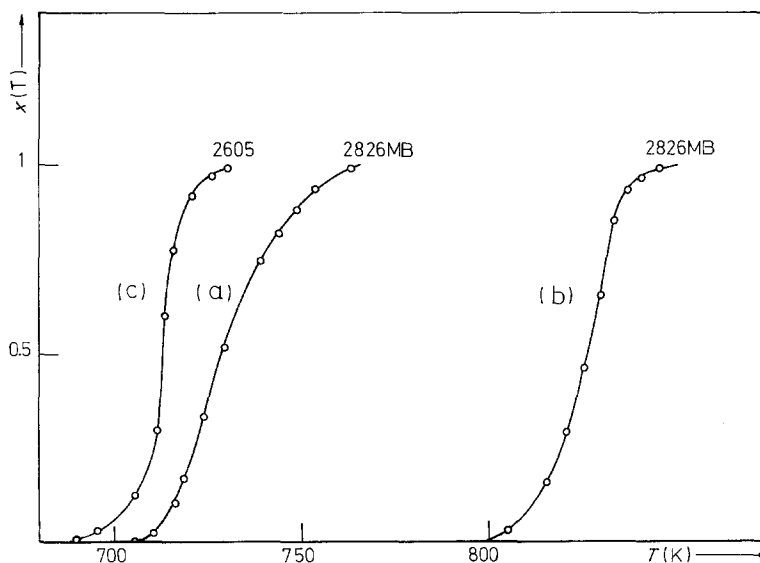
Figure 7 Temperature dependence of crystallized fraction for (a) and (b) 2826 MB, and (c) 2605 alloys.

2826 A ($Fe_{32}Ni_{36}Cr_{14}P_{12}B_6$) [18]. One notices that for the first stage the values are very similar (3.04 eV at^{-1} for 2826 A) and that should be consistent with the similarity between both processes. Activation energies for the second stage are higher than that corresponding to the first stage in both materials and the greater value for 2826 A (4.7 eV at^{-1}) could be assigned to the presence of phosphorus. This trend was first observed by Orehotsky [12] in the Fe–P–B system: activation energies became larger as phosphorus replaced boron in the alloys, and after by Boswell [20] in the Ni–Pd–P system.

The lower activation energy for the 2605 alloy can be explained by an acceleration of the crystallization associated with the quenched-in nuclei present in the as-received ribbons, as reported elsewhere [17].

4.2. Electrical resistivity

Our analysis of crystallization kinetics from isothermal resistivity measurements is based on the method developed by Germain et al. [21–25]. In this method the crystallized fraction is defined by

$$x(t) = 1 - \exp\left(-\frac{V(t)}{V_0}\right),$$

$V(t)$ being the "extended crystallized volume" and V_0 the total volume. $x(t)$ can be obtained from the conductivity σ_m of the sample through the Landauer formula [26]

$$\ln\left(\frac{1}{1-x}\right) = \ln\left[1 - \left(\frac{\sigma_a - \sigma_m}{\sigma_a + 2\sigma_m}\right)\left(\frac{\sigma_c - \sigma_m}{\sigma_c + 2\sigma_m}\right)^{-1}\right]$$

if the conductivities σ_a and σ_c of amorphous and crystalline fractions are known. The time variation of $\ln(1/1-x)$ can be fitted by a fourth-order polynomial expression and the power of the highest coefficient indicates the most important crystallization regimen. This power r can be obtained as the slope of a straight line in a plot $\log[\ln(1/1-x)]$ versus $\log t$.

For bulk-induced crystallization there are two types of crystallites: (i) those, due to homogeneous nucleation, which are created throughout the time crystallization takes place, and (ii) those, existing before crystallization begins due to heterogenous nucleation (they exist in the amorphous state or are produced during heating up to the crystallization temperature). A critical time τ is defined as the time necessary for a growing crystallite to reach the surface and to change from a spherical growth to a cylindrical growth. The time variation of $\ln(1/1-x)$ for $t < \tau$ can be expressed in the form

$$\ln\frac{1}{1-x} = \frac{4}{3}\frac{p\pi}{S}(a_0 + v_G t)^3 + \frac{\pi}{3}nv_G^3 t^4,$$

according to Germain et al. [24], where p and a_0 are the number and the mean size of the initial crystallites, v_G their growth rate, S the surface of the layer, and n the nucleation rate.

It is established [1] that 2826 MB alloy crystallizes in two stages. During the first stage γ(Fe–Ni) austenitic crystallites are formed by a primary crystallization mechanism and thus the boron concentration of the amorphous matrix increases continuously from 18% to 25%.

An extensive study of nucleation rates and the time evolution of diameters for these primary crystals have been done using HVEM microscopy by the authors [27]. A parabolic growth is observed in all cases, but only for very short times (< 20 min), and then a linear dependence is established. This second zone should correspond to the overlapping of diffusion fields because of the very high nucleation rate of these crystallites before impingement occurs. This time approximately corresponds to the induction time of the experiments and, therefore, a constant growth rate can be assumed.

One also notices that σ_a is not strictly constant for the first stage because of the boron rejected from the growing crystallites. However, we think that the inaccuracy involved in this assumption is negligible because it has been well established [28–30] that for analogous systems resistivity increases only slightly when metalloid concentration changes in the range 12% to 40% and then a rapid increase is observed. From Stobiecki and Hoffmann's work [28] we draw the conclusion that the change in σ_a is less than 5%.

Moreover Landauer's equation is only strictly correct if we assume some hypothesis but can be roughly extended to other cases and is nevertheless a very good approximation [26]. On the other hand, the use of the Landauer's equation in our case is supported by the agreement between experimental measurements and theoretical values obtained on the basis of crystallized fractions evaluated from TEM experiments.

The results obtained for 2826 MB alloy are given in Fig. 8. Runs performed at 665 and 675 K
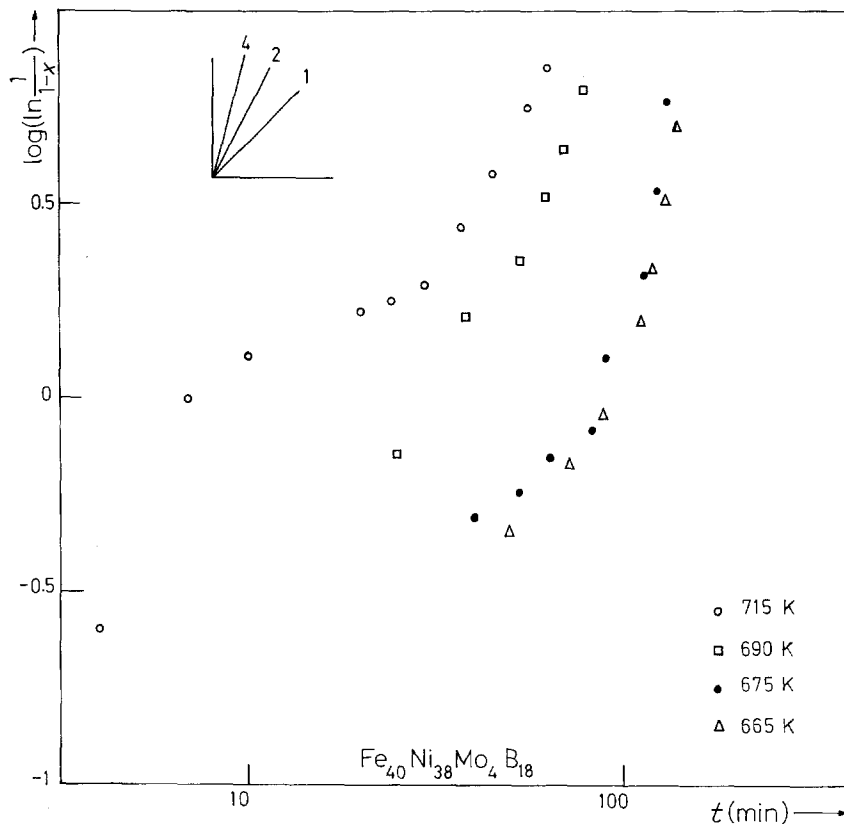
Figure 8 Time variation of ln $(1/1 - x)$ for 2826 MB alloy. The inset plot illustrates the different slopes.

have very similar characteristics: for small times $(t < 70\,\text{min})$ $r \sim 1$; for $t > 70\,\text{min}$ the possible value of r nearest to the experimental slope is 4. The proximity of the crystallization conclusion $(x \to 1)$ attaches a greater uncertainty on $1/1 - x$ and that should explain the differences between experimental and theoretical values. The following interpretation can be offered: (a) for small times the heterogeneous nucleation predominates over homogeneous nucleation and, because v_G is small, the linear term is the most important; (b) in a second period of time, r increases up to $r \sim 4$, because the contribution to the crystallite fraction due to homogeneous nucleation becomes preponderant. For $t > \tau$ crystallization is completed as indicated by electron diffraction patterns [1].

For samples crystallized at higher temperatures, a different behaviour is observed. A run performed at 690 K shows a value $r \sim 2$ for all times, but for 715 K, near the onset of crystallization, the slope drops (falls) from 2 to a value close to 0 in the 10 min $< t <$ 30 min interval. For these temperatures a high number of embryos are formed during the induction time and heterogeneous nucleation

occurs. Homogeneous nucleation remains negligible at all times, and crystallization is dominated by the growth of the large initial crystallites.

Justification of the validity of the above interpretation is supplied by electron microscopy. In our study [1] of the crystallization of this material, two metastable crystalline phases are detected and, for the higher temperature, the very small MSI crystals which have been nucleated first are not dissolved, but remain and become enclosed by the much bigger MSII crystals. At 715 K we have observed in TEM the formation of elliptical or spherical MSII crystals, at the induction time, rapidly growing to reach the surface. The contribution of MSII crystal dominates the crystallization and a two-dimensional phase-boundary-controlled growth, giving a t^2 law, is expected. The short intermediate stage with $r \sim 0$ detected in the run performed at 715 K could be explained by the polygonization phenomenon observed in TEM in which a crystallographic rearrangement occurs but the crystallized fraction does not change.

For the 2605 alloy, Fig. 9 shows logarithmic
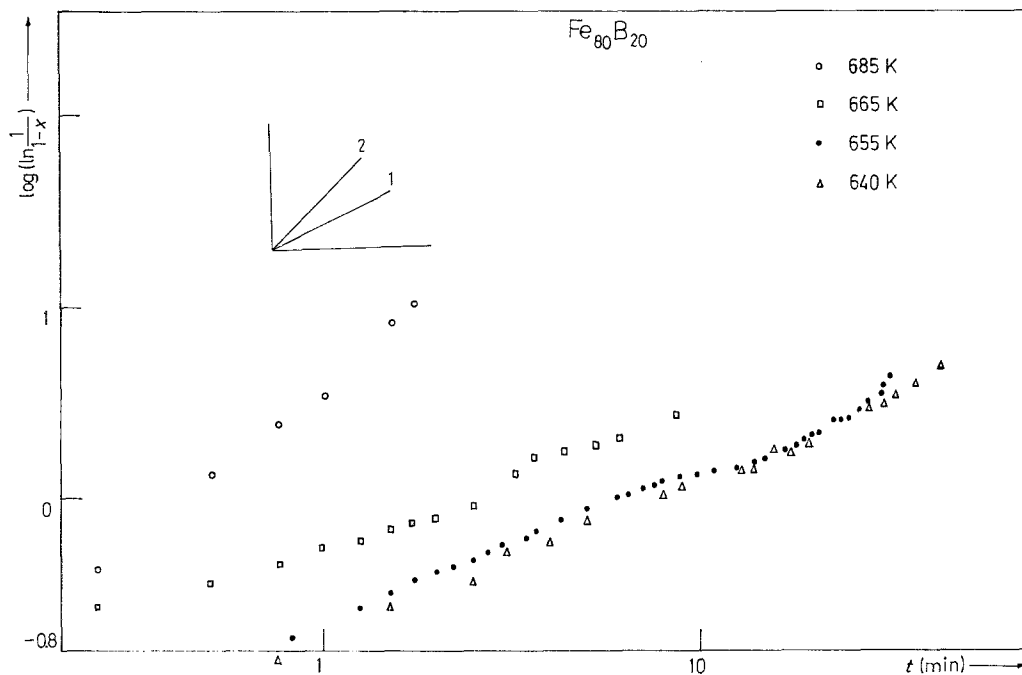
Figure 9 Time variation of ln $(1/1 - x)$ for 2605 alloy. The inset plot illustrates the different slopes.

plots of $\ln(1/1 - x)$ against time for different annealing temperatures. In the temperature range explored, a single crystallization stage is found. For the three lower temperatures a value $r \sim 1$ results but, for the highest temperature, $r \sim 2$. The existence of a single stage could be explained as follows: as known, two different crystalline phases (α-Fe and Fe_3B) are formed in the crystallization of the $Fe_{80}B_{20}$ system [31]. For alloys containing 16 at.% of more boron, crystallization has been observed to occur by a eutectoid reaction producing both phases simultaneously [31].

From previous results and our observations it is known that the shape common to all the eutectic crystals is that of a cylinder with rounded ends and a characteristic fine structure. The one-dimensional growth of cylinders to reach the ribbon surface is consistent with the observed value $r \sim 1$. On the other hand, the crystallization starts near that side of the ribbon which has not been in contact with the rotating wheel during production of the ribbon [32] and progresses towards the opposite surface. This effect agrees with the "surface-induced crystallization" model proposed by Germain *et al.* [19, 20] and provides supplementary arguments to the above assumptions. For annealing temperatures near the crystallization onset, the two-dimensional expansion of cylinders could explain the observed value $r \sim 2$.

A previous kinetic study of this material [33] reported higher values of r; however, a direct comparison is not possible because of the different definition of crystallized fraction. In spite of this, the small values of the induction time reported by Tóth [33] should indicate preponderant homogeneous nucleation of α-Fe precipitates in the very first stages of crystallization.

5. Conclusion

We can conclude from the above observations by different experimental techniques that crystallization in $Fe_{40}Ni_{38}Mo_4B_{18}$ Metglas proceeds through two stages: in the first stage the process is dominated by a primary precipitation with a very high nucleation rate. Heterogeneous nucleation plays an important role in this stage because of the quenched-in nuclei present or by embryos formed during induction time in isothermal experiments. The second stage, involving the higher activation energy, is dominated by the two-dimensional phase-boundary growth of the coarser MSII crystals.

Crystallization in the $Fe_{80}B_{20}$ system proceeds by the separation of two phases which requires only short-range diffusion. The cylindrical shape common to all eutectic crystals is an important structural feature in order to explain the crystallization kinetics.

2685

Interpretation of kinetics from electrical resistivity measurements agree with TEM observations previously reported.

References

1. F. L. CUMBRERA, M. MILLAN, P. VIGIER, A. CONDE and R. MARQUEZ, *J. Mater. Sci.* 17 (1982) 861.
2. L. J. VAN DER PAUW, *Philips Res. Reports* 13 (1958) 1.
3. L. B. VALDES, *Proc. I.R.E.* 42 (1954) 420.
4. J. DURAND and M. YUNG, "Amorphous magnetism I" (Plenum Press, New York, 1977) p. 275.
5. J. J. BECKER, F. E. LUBORSKY and J. L. WALTER, *IEEE Trans. Magn.* MAG-13 (1977) 988.
6. R. C. O'HANDLEY, R. HASEGAWA, R. RAY and P. CHOU, *Appl. Phys. Lett.* 29 (1976) 330.
7. A. K. MAJUMDAR and A. K. NIGAM, *J. Appl. Phys.* 51 (1980) 4218.
8. U. HEROLD, U. KÖSTER and A. G. DIRKS, *Soft Magnetic Materials 4, Euphysics Conference Abstracts* 3E (1979) 94.
9. Y. KHAN and M. SOSTARICH, *Z. Metallkde* 72 (1981) 266.
10. T. KEMENY, I. VINCZE and B. FOGARASSY, *Phys. Rev. B* 20 (1979) 476.
11. R. MALMHALL, S. M. BHAGAT, K. V. RAO and G. BÄCKSTROM, *Phys. Stat. Sol. (a)* 53 (1979) 641.
12. J. OREHOTSKY, *J. Appl. Phys.* 50 (1979) 7612.
13. J. W. CHRISTIAN, "The Theory of Transformations in Metals and Alloys", 2nd edn. (Pergamon Press, Oxford, 1975) Part 1.
14. A. LUCCI and M. TAMANINI, *Thermochim. Acta* 13 (1975) 147.
15. L. BATTEZATTI, A. LUCCI and G. RIONTINO, *Thermochim. Acta* 23 (1978) 213.
16. H. E. KISSINGER, *Analy. Chem.* 29 (1957) 1703.
17. J. A. LEAKE and A. L. GREER, *J. Non-Cryst. Sol.* 38/39 (1980) 735.
18. M. VON HEIMENDAHL and G. KUGLSTATTER, *J. Mater. Sci.* 16 (1981) 2405.
19. R. S. TIWARI, S. RANGANATHAN and M. VON HEiMENDAHL, *Z. Metallkde* 72 (1981) 563.
20. P. G. BOSWEEL, *Script. Metal.* 11 (1977) 701.
21. P. GERMAIN, S. SQUELARD, J. C. BOURGOIN and A. GHEORGHIU, *J. Non-Cryst. Solids* 23 (1977) 93.
22. A. GHEORGHIU, S. SQUELARD, K. ZELLAMA, P. GERMAIN and J. C. BOURGOIN, *Phys. Rev. Appl.* 12 (1977) 721.
23. P. GERMAIN, S. SQUELARD, J. C. BOURGOIN and A. GHEORGHIU, *J. Appl. Phys.* 48 (1977) 1909.
24. P. GERMAIN, K. ZELLAMA, S. SQUELARD and J. C. BOURGOIN, *J. Appl. Phys.* 50 (1979) 6986.
25. K. ZELLAMA, P. GERMAIN, S. SQUELARD, J. C. BOURGOIN and P. A. THOMAS, *J. Appl. Phys.* 50 (1979) 6995.
26. R. LANDAUER, *J. Appl. Phys.* 23 (1952) 779.
27. F. L. CUMBRERA, *Portug. Phys.*, in press.
28. R. STOBIECKI and H. HOFFMANN, *J. Phys.* C8 (1980) 485.
29. P. J. COTE, *Sol. State. Commun.* 18 (1976) 1311.
30. B. Y. BUCHER, *J. Non-Cryst. Solids* 7 (1972) 277.
31. J. L. WALTER, S. F. BARTRAM and R. R. RUSSEL, *Met. Trans. A* 9 (1978) 803.
32. U. KOSTER and U. HEROLD, *Script. Metal.* 12 (1978) 75.
33. J. TOTH, *Mat. Res. Bull.* 13 (1978) 691.